



ChemComm

**A Strategy to Improve the Performance of Cerium(III)  
Photocatalysts**

Journal:	<i>ChemComm</i>
Manuscript ID	CC-COM-01-2019-000282.R1
Article Type:	Communication

SCHOLARONE™  
Manuscripts

## A Strategy to Improve the Performance of Cerium(III) Photocatalysts

Yusen Qiao, Thibault Cheisson, Brian C. Manor, Patrick J. Carroll, and Eric J. Schelter\*

 Received 00th January 20xx,  
 Accepted 00th January 20xx

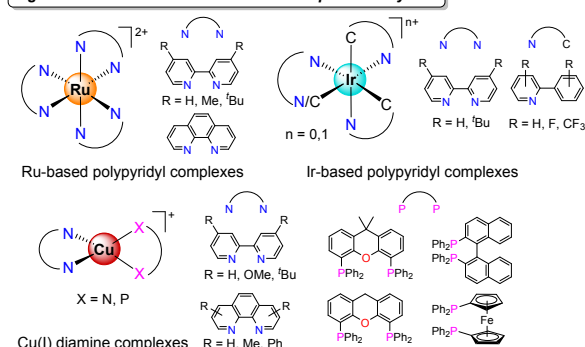
DOI: 10.1039/x0xx00000x

[www.rsc.org/](http://www.rsc.org/)

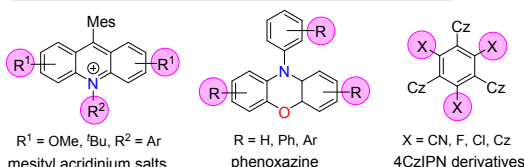
A structural modification strategy to improve the photocatalytic performance of a series of cerium(III) *bis*(guanidinate) *mono*(amide) molecular luminophores was demonstrated. Reducing the steric bulkiness of the amide ligand gave rise to two categories of complexes with distinct photophysical and photochemical properties. A structural parameter, the amide cone angle ( $\theta$ ), was applied to differentiate the two categories. Complexes with smaller cone angles ( $\theta < 156^\circ$ , category B) exhibited more reducing potentials and faster electron-transfer rates than those of complexes with larger cone angles ( $\theta > 173^\circ$ , category A). And only complexes in the category B could achieve the photocatalytic phenylation of an aryl bromide. These results demonstrated that reducing the steric bulkiness of the amide ligand improved the performance of cerium(III) *bis*(guanidinate) *mono*(amide) photocatalysts in a synthetic manner.

Significant research efforts have been devoted to the development of efficient and practical photocatalysis.<sup>1, 2</sup> Investigations of transition-metal photocatalysts, such as Ru- and Ir-based polypyridyl complexes, have been crucial to recent advancements in photoredox catalysis (Fig. 1).<sup>1, 2</sup> These photocatalysts can generate reactive intermediates from a variety of organic substrates, from their ability to absorb visible light and initiate electron- or energy transfer reactions from reactive excited states. The excited-state redox properties of these catalysts are tuned by ligand modifications.<sup>3, 4</sup> For example, adding electron-withdrawing substituents, such as fluoride or trifluoromethyl groups, to the phenylpyridine ligands in Ir(III) photocatalysts increase the Ir<sup>3+/4+</sup> oxidation potential.<sup>3</sup> Such ligand modifications generate stronger iridium photooxidants with better catalytic efficiencies.<sup>2</sup>

### Ligand modifications for transition-metal photocatalysts



### Electronic density modifications for organic photocatalysts



### This work: ligand steric modifications for cerium(III) photocatalysts

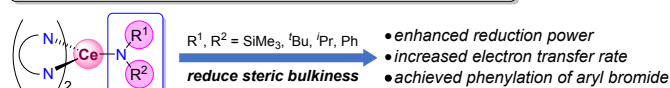


Fig. 1 Common approaches and our approach to tailor photocatalysts.

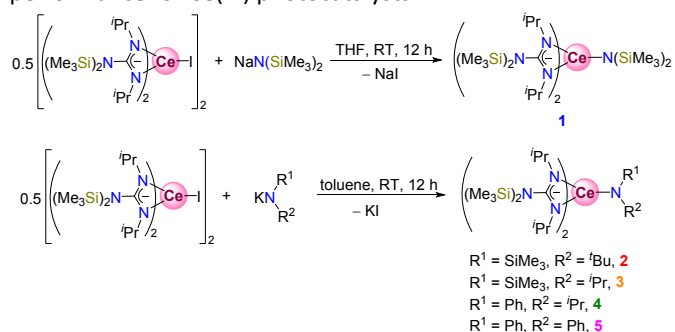
Recently, there has been a motivation to develop earth-abundant metal and organic photocatalysts as complementary reactive species to Ru/Ir photocatalysts, in an effort to provide equal or better performance in organic synthesis, for the purposes of sustainable development.<sup>5-9</sup> Molecular design principles that improve the photochemical properties of earth-abundant metal and organic photocatalysts have been reported (Fig. 1).<sup>10-13</sup> For example, incorporating a BINAP (2,2'-bis(diphenylphosphino)-1,1'-binaphthyl) ligand increased the reduction power of a Cu(I)-based photocatalyst and afforded the best yield (87%) in a reductive decarboxylative C<sub>sp</sub><sup>3</sup>-C<sub>sp</sub> bond coupling reaction among fifty Cu(I)-based photocatalysts.<sup>10</sup> Modification of the electron density of phenoxazine

P. Roy and Diana T. Vagelos Laboratories, Department of Chemistry, University of Pennsylvania, 231 S 34th Street, Philadelphia, Pennsylvania 19104, USA. E-mail: schelter@sas.upenn.edu

† Electronic Supplementary Information (ESI) available: Synthetic details and characterizations; electronic absorption, excitation, and emission data; electrochemical data; computational details; X-ray crystallographic data. CCDC 1883150–1883153. See DOI: 10.1039/x0xx00000x

photocatalysts was used to alter triplet energies and excited-state redox potentials to achieve high conversions while maintaining good control of dispersity (< 1.3) over the entire duration of methyl methacrylate polymerizations.<sup>13</sup>

Our group initiated development of earth-abundant lanthanide photocatalysts, especially for cerium.<sup>14–19</sup> Our group have incorporated cerium photocatalysts into C(sp<sup>3</sup>)-C(sp<sup>3</sup>) and C(sp<sup>2</sup>)-C(sp<sup>2</sup>) bond forming reactions,<sup>17, 18</sup> as well as dehalogenation and borylation of unactivated aryl chlorides.<sup>16, 19</sup> Cerium photocatalysis has also been applied in dehydrogenation of amines,<sup>20</sup> C–C bond cleavage and amination of alkanols,<sup>21, 22</sup> and C–H activation of alkanes.<sup>23</sup> Structure-photophysics correlations, in terms of emission colors and brightness, have been established for molecular Ce(III) luminophores.<sup>15</sup> Despite the emerging applications of cerium photocatalysis in organic synthesis, strategies to control their reactivity have not yet been clearly elucidated. Herein, we describe a series of Ce(III) *bis*(guanidinate) *mono*(amide) complexes (**1–5**) and their structural, electrochemical, photophysical, and photochemical characteristics. Syntheses, structures, and catalytic applications of rare earth *bis*(guanidinate) *mono*(amide) complexes have been reported.<sup>24–27</sup> We hypothesized that the *bis*(guanidinate) *mono*(amide) ligand framework, which has been applied to provide a good quantum yield (79%) and relatively slow non-radiative decay rates compared to related Ce(III) luminophores,<sup>15, 18</sup> would allow us to modify the amide ligand substituents without quenching Ce(III) luminescence. And the electron-donating guanidinate and amide ligands would engender more reducing Ce(III) complexes. The goal here was to elucidate a structural modification approach to improve the performance for Ce(III) photocatalysts.



**Scheme 1** Synthesis of Ce(III) *bis*(guanidinate) *mono*(amide) complexes **1–5**.

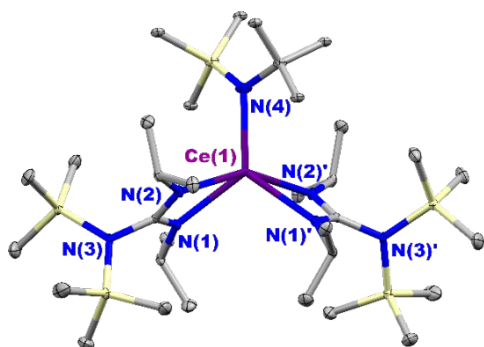


**Fig. 2** Thermal ellipsoid plot of **2** at 30% probability level.

The Ce(III) *bis*(guanidinate) *mono*(amide) complexes described in this study were prepared by salt metathesis between a Ce(III) *bis*(guanidinate) iodide starting material,  $\{[(\text{Me}_3\text{Si})_2\text{N}(\text{N}^{\text{Pr}})_2]_2\text{Ce}\}_2(\mu^2\text{---})_2$ ,<sup>18</sup> and alkali metal salts of amide ligands,  $\text{MNR}^1\text{R}^2$  ( $\text{M} = \text{Na}$  for **1**, or  $\text{K}$  for **2–5**), in THF (for **1**)<sup>18</sup> or toluene (for **2–5**) at room temperature (Scheme 1). All complexes were crystallized from saturated *n*-pentane solutions at  $-25^\circ\text{C}$  and isolated in ca. 50% yields (see section 2 in the ESI† for details). Complexes **1–5** were characterized by X-ray diffraction studies (Fig. 2 and S6–S9). We found that the cone angles ( $\vartheta$ ) of the amide moieties ( $-\text{NR}^1\text{R}^2$ )<sup>28</sup> decreased from ca.  $170^\circ$  for **1** and **2** to ca.  $150^\circ$  for **3–5**, and complexes **1–5** could be divided into two categories based on their cone angles: complexes **1** and **2** ( $\vartheta > 173^\circ$ , category **A**), and complexes **3–5** ( $\vartheta < 156^\circ$ , category **B**) (Table 1, see the section 10 in the ESI†). The photophysical and photochemical properties of **1–5** were evaluated next to detect the impact of the structural change.

**Table 1** The cone angles ( $\vartheta$ ), Ce<sup>III/IV</sup> reduction potentials ( $E_{1/2}$ ), and quenching rates ( $k_q$ ) with 4-bromofluorobenzene of **1–5**. Standard deviations were given in parentheses. Complexes are divided into two categories (**A** and **B**) based on their cone angles.

compound	category	$\vartheta$ ( $^\circ$ )	$E_{1/2}$ (V)	$k_q$ ( $\times 10^7 \text{ M}^{-1} \text{ s}^{-1}$ )
<b>1</b>	<b>A</b>	173.87	−0.14	0.43(1)
<b>2</b>	<b>A</b>	173.56	−0.26	0.41(1)
<b>3</b>	<b>B</b>	147.41	−0.41	1.0(1)
<b>4</b>	<b>B</b>	155.78	−0.57	2.2(1)
<b>5</b>	<b>B</b>	146.68	−0.56	5.3(1)

Electronic absorption spectra of complexes **1–5** were collected in toluene at room temperature (Fig. 3). The spectra displayed two bands with  $\epsilon \sim 10^2 \text{ M}^{-1} \text{ cm}^{-1}$  for **1–3**. The higher energy band ( $\lambda_{\text{abs}}^2$ ) was at ca. 350 nm and the lower energy band ( $\lambda_{\text{abs}}^1$ ) was red-shifted from 429 nm for **1** to 463 nm for **3**. The spectra for **4** and **5** only displayed the  $\lambda_{\text{abs}}^1$  at ca. 460 nm. The  $\lambda_{\text{abs}}^2$  of **4** and **5** overlapped with higher energy bands that were tentatively assigned as ligand-to-metal charge transfer (LMCT) bands.<sup>15</sup> The molar extinction coefficients ( $\epsilon$ ) and the full width at half maxima (FWHM) of the  $\lambda_{\text{abs}}^1$  and  $\lambda_{\text{abs}}^2$  bands were consistent with the reported values of Ce(III)  $4f \rightarrow 5d$  transitions (Table S1).<sup>15, 19, 29–32</sup> The assignment of  $4f \rightarrow 5d$  transitions was further supported by time-dependent density functional theory (TD-DFT) calculations and natural transition orbitals (NTOs) analyses (see section 9 in the ESI† for details).<sup>33, 34</sup> The  $\lambda_{\text{abs}}^1$  was assigned to a  $4f \rightarrow 5d_z^2$  transition, whereas the  $\lambda_{\text{abs}}^2$  was assigned to a  $4f \rightarrow 5d_{xz}$  or  $4f \rightarrow 5d_{yz}$  transition.<sup>15, 18</sup> The red shift of  $\lambda_{\text{abs}}^1$  was consistent with the decrease in energy of the  $4f \rightarrow 5d_z^2$  transition from 3.01 eV (412 nm) for **1**<sup>15</sup> to 2.82 eV (440 nm) for **5**. The TD-DFT calculations overestimated the energies of the  $\lambda_{\text{abs}}^2$  bands, therefore the computed  $\lambda_{\text{abs}}^2$  bands of **1–5** overlapped with higher energy LMCT bands in the calculated absorption spectra. Moreover, complexes in the category **B** exhibited lower energy  $\lambda_{\text{abs}}^1$  bands (ca. 460 nm) compared to those of complexes in the category **A** (ca. 430 nm) (Fig. S61, ESI†).

All complexes were luminescent and demonstrated a range of emission colors: green for **1** and **2**, yellow for **3**, and lime green for **4** and **5**. The different emission colors resulted from the different Stokes shifts between **1–5**. The Stokes shift for **3** (112 nm) was larger than those for the other complexes (ca. 80 nm), presumably due to the larger geometric relaxation after the excitation for **3**.<sup>15</sup> The emission bands for all complexes were fit by two Gaussian bands, corresponding to  ${}^2\text{D} \rightarrow {}^2\text{F}_{5/2}$  and  ${}^2\text{D} \rightarrow {}^2\text{F}_{7/2}$  transitions (Fig. S18–S21, ESI†).<sup>15</sup> Complexes in the

category **B** exhibited lower energy emission bands compared to those of complexes in the category **A** (Fig. S62, ESI<sup>†</sup>).

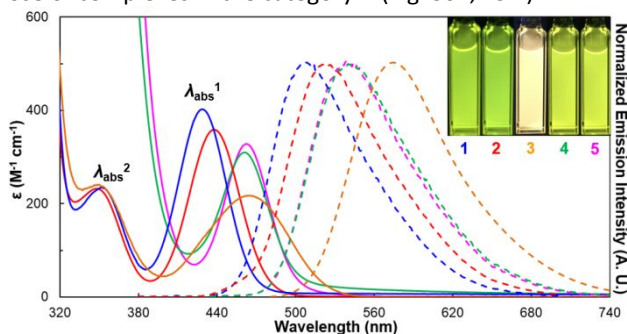


**Fig. 3** Absorption (solid lines) and emission spectra (dashed lines) of **1** (blue), **2** (red), **3** (yellow), **4** (green), and **5** (pink). Inset: images of toluene solutions of **1–5** in 1 cm path length quartz cuvettes (1.0 mM) under 365 nm UV irradiation. The spectra were collected in toluene. The  $\lambda_{\text{abs}}^1$  and  $\lambda_{\text{abs}}^2$  bands were assigned in the absorption spectra.

Lifetimes ( $\tau$ ) and photoluminescence quantum yields ( $\phi_{\text{PL}}$ ) were obtained in toluene at room temperature (Table S1, ESI<sup>†</sup>). The lifetimes for the <sup>2</sup>D excited states of **1** (117 ns), **2** (221 ns), **3** (158 ns), **4** (41 ns), and **5** (43 ns) were consistent with reported lifetimes for molecular Ce<sup>III</sup> emitters.<sup>15, 29–32</sup> The quantum yields were found to increase from **5** (0.10), **4** (0.14), and **3** (0.23) to **2** (0.75) and **1** (0.79). The increase of quantum yields was consistent with the increase of amide cone angles ( $\theta$ )<sup>28</sup> from ca. 150° for the category **A** to ca. 170° for the category **B** (Fig. S63).

Cyclic voltammetry (CV) experiments of complexes **1–5** were conducted at ambient temperature in CH<sub>2</sub>Cl<sub>2</sub> and demonstrated quasi-reversible Ce<sup>III/IV</sup> redox features (Fig. S26–S30, ESI<sup>†</sup>). The ground-state Ce<sup>III/IV</sup> reduction potentials ( $E_{1/2}$ ) were determined to be –0.14 V, –0.26 V, –0.41 V, –0.57 V, and –0.56 V versus Cp<sub>2</sub>Fe<sup>0/+</sup> for **1**, **2**, **3**, **4**, and **5**, respectively (Table 1). Complexes **2–5** were more reducing than our previous Ce(III) guanidinate–amide complexes ( $E_{1/2} = +0.05$  V to –0.22 V versus Cp<sub>2</sub>Fe<sup>0/+</sup>).<sup>18</sup> To explore the role of ligand modification in affecting the cerium reduction potentials, we computed the electronic structures for **1–5** by DFT calculations (see section 9 in the ESI<sup>†</sup> for details). The optimized structures were in good agreement with the crystallographically determined bond lengths and bond angles. While the lowest unoccupied molecular orbital (LUMO) energy for all complexes remained mostly unaffected by the ligand modifications, the highest occupied molecular orbitals (HOMO) energy was found to increase from –5.03 eV for **1** to –4.54 eV for **5** (Table S11, ESI<sup>†</sup>). Moreover, a linear correlation was established between the  $E_{1/2}$  and the HOMO energy for **1–5**: compounds with higher HOMO energies had more reducing  $E_{1/2}$  values (Fig. S57, ESI<sup>†</sup>). Similar HOMO–energy to reduction–potential correlations have been observed in a series of Fe(depe)<sub>2</sub>(N<sub>2</sub>) complexes (depe = 1,2-bis(diethylphosphino)–ethane)<sup>35</sup> and tungsten–alkylidene complexes.<sup>36</sup> A linear LUMO energy–reduction potential correlation for Ce(IV) complexes was established by our group.<sup>37</sup> For the current series, we observed a relationship between the HOMO energies and the cone angles: compounds with smaller cone angles (category **B**) exhibited higher HOMO energies (Fig. S64, ESI<sup>†</sup>) and thereby more reducing potentials (Fig. S65, ESI<sup>†</sup>) than those of compounds with larger cone angles (category **A**). An important finding here was that even though

the amide ligands in **1** (pK<sub>a</sub> = 30 in DMSO), **2** (pK<sub>a</sub> = 34 in THF), and **3** (pK<sub>a</sub> = 31 in THF) were more electron-rich than that in **5** (pK<sub>a</sub> = 25 in DMSO),<sup>38, 39</sup> the reduction potential of **5** was more reducing than those of **1–3**, which was the opposite result that would be expected on the basis of electronic effects alone. While the pK<sub>a</sub> of the amide ligand in **4** (pK<sub>a</sub> ≈ 31 in DMSO) was higher than that in **5** (pK<sub>a</sub> = 25 in DMSO),<sup>38, 39</sup> complexes **4** and **5** exhibited similar absorption and emission spectra, HOMO energies, and reduction potentials. Moreover, DFT calculations demonstrated that introducing fluoride or methoxy groups at the *para* positions of the phenyl rings in complex **5** did not significantly impact the energies of the 4f→5d<sub>2</sub> transitions and the Ce<sup>III/IV</sup> reduction potentials (see section 9 in the ESI<sup>†</sup> for details). Consequently, we postulated that the physical properties of complexes **1–5** were governed by the steric effects instead of the electronic effects. We next investigated the excited-state photochemistries for **1–5**.

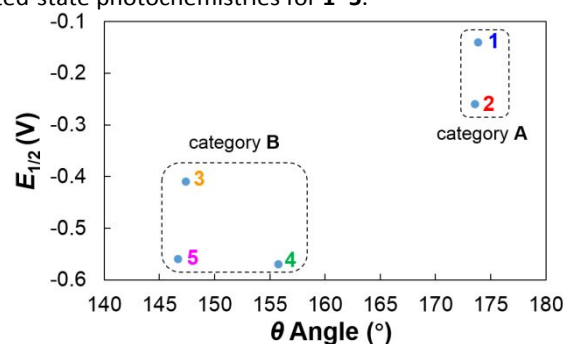
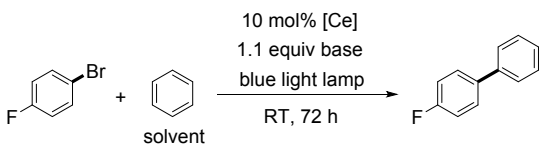


**Fig. 4** A plot of the cone angles ( $\theta$ ) and the reduction potentials ( $E_{1/2}$ ) for complexes **1–5**. The dashed box is used to indicate two categories of compounds.

The excited-state reduction potentials ( $E_{1/2}^*$ ) were estimated to be –2.6, –2.6, –2.6, –2.9, and –2.9 V versus Cp<sub>2</sub>Fe<sup>0/+</sup> for **1**, **2**, **3**, **4**, and **5**, respectively, by the Rehm–Weller formalism.<sup>40, 41</sup> The  $E_{1/2}^*$  values of **4** and **5** approached the reduction potential of phenyl bromide ( $E_{\text{PhBr}^{\bullet-}/\text{PhBr}} = -2.89$  V versus Cp<sub>2</sub>Fe<sup>0/+</sup> in DMF)<sup>42</sup>, and **4** and **5** were more reducing than [Ru(bpy)<sub>3</sub>]<sup>2+</sup> ( $E_{1/2}^* \approx -1.21$  V versus Cp<sub>2</sub>Fe<sup>0/+</sup>), *fac*-Ir(ppy)<sub>3</sub> ( $E_{1/2}^* \approx -2.13$  V versus Cp<sub>2</sub>Fe<sup>0/+</sup>),<sup>43</sup> and the lanthanide reducing agent, SmI<sub>2</sub> in the presence of hexamethylphosphoramide (HMPA) ( $E_{1/2} = -2.31$  V versus Cp<sub>2</sub>Fe<sup>0/+</sup>).<sup>44</sup> Stern–Volmer experiments of **1–5** demonstrated moderately fast quenching rates ( $k_{\text{q}} \approx 10^6$ – $10^7$  M<sup>–1</sup> s<sup>–1</sup>) toward 4-bromofluorobenzene (Table 1). Complexes in the category **B** (**3–5**) exhibited faster quenching rates ( $1.0$ – $5.3 \times 10^7$  M<sup>–1</sup> s<sup>–1</sup>) than those of complexes in the category **A** (**1** and **2**,  $4.1$ – $4.3 \times 10^6$  M<sup>–1</sup> s<sup>–1</sup>) (Fig. S66, ESI<sup>†</sup>). Therefore, reducing the steric bulkiness of the amide moiety increased the interactions of the Ce 5d<sub>2</sub> excited states with the organic substrates.<sup>14</sup> The data indicated that complex **5** was the most potent photoreductant among the current series. To demonstrate that complex **5** was also the most efficient in photocatalysis, we compared the performance of **1–5** in the photocatalytic phenylation of 4-bromofluorobenzene (Table 2). No product was formed without Ce(III) complexes. The reactions with **1–5** were conducted under identical conditions, except for the use of different amide bases to maintain the identities of the Ce(III) catalysts. The yield of the phenylation product was significantly increased from 0% using **1** to 66% using **5**. Moreover, the yield using **5** (66%) was higher than that using the best catalyst in the previous Ce(III) guanidinate–amide

series,  $\text{Ce}[\text{N}(\text{SiMe}_3)_2]_3$  (32%).<sup>18</sup> And only the complexes in the category **B** achieved phenylation of aryl bromides (yields: 12–66%), whereas complexes in the category **A** basically showed no reactivity with aryl bromides (Table 2).

**Table 2** Phenylation of 4-bromofluorobenzene by 1–5.<sup>a</sup>



entry	[Ce] catalyst	base	yield (%)
1	1	$\text{KN}(\text{SiMe}_3)_2$	0 <sup>b</sup>
2	2	$\text{KN}(\text{SiMe}_3)(\text{tBu})$	< 5 <sup>b</sup>
3	3	$\text{KN}(\text{SiMe}_3)(i\text{Pr})$	12 <sup>c</sup> (18) <sup>b</sup>
4	4	$\text{KN}(\text{Ph})(i\text{Pr})$	36 <sup>c</sup> (43) <sup>b</sup>
5	5	$\text{KN}(\text{Ph})_2$	66 <sup>c</sup> (70) <sup>b</sup>
6	-	$\text{KN}(\text{Ph})_2$	0 <sup>b</sup>

<sup>a</sup>standard conditions: 0.2 mmol 4-bromofluorobenzene, 0.02 mmol (10 mol%) Ce catalyst, 0.22 mmol base, 2 mL benzene, irradiated by a 34 W blue light lamp with fan cooling at room temperature for 72 h. <sup>b</sup>yield (conversion) was determined by <sup>19</sup>F NMR spectroscopy with *p*-fluorotoluene as an internal standard. <sup>c</sup>isolated yield.

In summary, we demonstrated that altering the steric bulkiness of the amide ligand resulted in two categories of Ce(III) *bis*(guanidinate) *mono*(amide) luminophores with distinct photophysical and photochemical properties. Complexes with smaller amide ligands exhibited more reducing potentials, faster electron-transfer rates, and improved efficiency for the photocatalytic phenylation of an aryl bromide. We are currently employing the structural modification approach to design more potent lanthanide photocatalysts to activate challenging organic substrates.

This material is based upon work supported by the U.S. Department of Energy, Office of Science, Office of Basic Energy Sciences, Separation Science program under Award Number DE-SC0017259. This work used the Extreme Science and Engineering Discovery Environment (XSEDE), which is supported by U.S. National Science Foundation Grant Number ACI-1548563. The Petersson and Chenoweth groups at the University of Pennsylvania are thanked for use of their fluorimeters. Dr. Robert Higgins is acknowledged for helpful discussions.

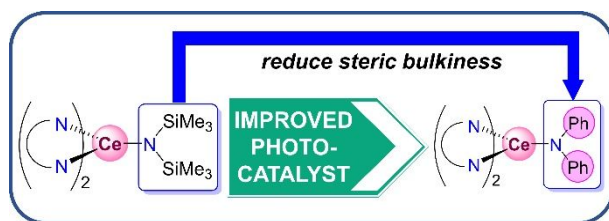
## Conflicts of interest

There are no conflicts to declare.

## Notes and references

- J. M. R. Narayanam and C. R. J. Stephenson, *Chem. Soc. Rev.*, 2011, **40**, 102–113.
- C. K. Prier, D. A. Rankic and D. W. C. MacMillan, *Chem. Rev.*, 2013, **113**, 5322–5363.
- I. M. Dixon, J.-P. Collin, J.-P. Sauvage, L. Flamigni, S. Encinas and F. Barigelletti, *Chem. Soc. Rev.*, 2000, **29**, 385–391.
- K. Teegardin, J. I. Day, J. Chan and J. Weaver, *Organic Process Research & Development*, 2016, **20**, 1156–1163.
- O. S. Wenger, *J. Am. Chem. Soc.*, 2018, **140**, 13522–13533.
- N. A. Romero and D. A. Nicewicz, *Chem. Rev.*, 2016, **116**, 10075–10166.
- T. C. Jenks, M. D. Bailey, J. Hovey, S. Fernando, G. Basnayake, M. E. Cross, W. Li and M. J. Allen, *Chem. Sci.*, 2018, **9**, 1273–1278.
- R. F. Higgins, S. M. Fatur, S. G. Shepard, S. M. Stevenson, D. J. Boston, E. M. Ferreira, N. H. Damrauer, A. K. Rappé and M. P. Shores, *J. Am. Chem. Soc.*, 2016, **138**, 5451–5464.
- Y. Zhang, J. L. Petersen and C. Milsman, *J. Am. Chem. Soc.*, 2016, **138**, 13115–13118.
- C. Minozzi, A. Caron, J.-C. Grenier-Petel, J. Santandrea and S. K. Collins, *Angew. Chem. Int. Ed.*, 2018, **57**, 5477–5481.
- A. Joshi-Pangul, F. Lévesque, H. G. Roth, S. F. Oliver, L.-C. Campeau, D. Nicewicz and D. A. DiRocco, *J. Org. Chem.*, 2016, **81**, 7244–7249.
- E. Speckmeier, T. G. Fischer and K. Zeitler, *J. Am. Chem. Soc.*, 2018, **140**, 15353–15365.
- B. G. McCarthy, R. M. Pearson, C.-H. Lim, S. M. Sartor, N. H. Damrauer and G. M. Miyake, *J. Am. Chem. Soc.*, 2018, **140**, 5088–5101.
- Y. Qiao and E. J. Schelter, *Acc. Chem. Res.*, 2018, **51**, 2926–2936.
- Y. Qiao, D.-C. Sergentu, H. Yin, A. V. Zabula, T. Cheisson, A. McSkimming, B. C. Manor, P. J. Carroll, J. M. Anna, J. Autschbach and E. J. Schelter, *J. Am. Chem. Soc.*, 2018, **140**, 4588–4595.
- Y. Qiao, Q. Yang and E. J. Schelter, *Angew. Chem. Int. Ed.*, 2018, **57**, 10999–11003.
- H. Yin, P. J. Carroll, J. M. Anna and E. J. Schelter, *J. Am. Chem. Soc.*, 2015, **137**, 9234–9237.
- H. Yin, P. J. Carroll, B. C. Manor, J. M. Anna and E. J. Schelter, *J. Am. Chem. Soc.*, 2016, **138**, 5984–5993.
- H. Yin, Y. Jin, J. E. Hertzog, K. C. Mullane, P. J. Carroll, B. C. Manor, J. M. Anna and E. J. Schelter, *J. Am. Chem. Soc.*, 2016, **138**, 16266–16273.
- K. Suzuki, F. Tang, Y. Kikukawa, K. Yamaguchi and N. Mizuno, *Angew. Chem. Int. Ed.*, 2014, **53**, 5356–5360.
- J.-J. Guo, A. Hu, Y. Chen, J. Sun, H. Tang and Z. Zuo, *Angew. Chem. Int. Ed.*, 2016, **55**, 15319–15322.
- A. Hu, J.-J. Guo, H. Pan, H. Tang, Z. Gao and Z. Zuo, *J. Am. Chem. Soc.*, 2018, **140**, 1612–1616.
- A. Hu, J.-J. Guo, H. Pan and Z. Zuo, *Science*, 2018, **361**, 668–672.
- Y. Zhou, G. P. A. Yap and D. S. Richeson, *Organometallics*, 1998, **17**, 4387–4391.
- M. V. Yakovenko, N. Y. Udilova, T. A. Glukhova, A. V. Cherkasov, G. K. Fukin and A. A. Trifonov, *New J. Chem.*, 2015, **39**, 1083–1093.
- P. Benndorf, J. Jenter, L. Zielke and P. W. Roesky, *Chem. Commun.*, 2011, **47**, 2574–2576.
- Z. Lu, G. P. A. Yap and D. S. Richeson, *Organometallics*, 2001, **20**, 706–712.
- J. A. Bilbrey, A. H. Kazez, J. Locklin and W. D. Allen, *J. Comput. Chem.*, 2013, **34**, 1189–1197.
- P. N. Hazin, J. W. Bruno and H. G. Brittain, *Organometallics*, 1987, **6**, 913–918.
- P. N. Hazin, C. Lakshminarayan, L. S. Brinen, J. L. Knee, J. W. Bruno, W. E. Streib and K. Folting, *Inorg. Chem.*, 1988, **27**, 1393–1400.
- M. D. Rausch, K. J. Moriarty, J. L. Atwood, J. A. Weeks, W. E. Hunter and H. G. Brittain, *Organometallics*, 1986, **5**, 1281–1283.
- X.-L. Zheng, Y. Liu, M. Pan, X.-Q. Lü, J.-Y. Zhang, C.-Y. Zhao, Y.-X. Tong and C.-Y. Su, *Angew. Chem. Int. Ed.*, 2007, **46**, 7399–7403.
- R. L. Martin, *J. Chem. Phys.*, 2003, **118**, 4775–4777.
- S. Tretiak, A. Saxena, R. L. Martin and A. R. Bishop, *Chem. Phys. Lett.*, 2000, **331**, 561–568.
- J. B. Geri, J. P. Shanahan and N. K. Szymczak, *J. Am. Chem. Soc.*, 2017, **139**, 5952–5956.
- B. Rudshiteyn, H. B. Vibbert, R. May, E. Wasserman, I. Warnke, M. D. Hopkins and V. S. Batista, *ACS Catal.*, 2017, **7**, 6134–6143.
- J. R. Levin, W. L. Dorfner, A. X. Dai, P. J. Carroll and E. J. Schelter, *Inorg. Chem.*, 2016, **55**, 12651–12659.
- F. G. Bordwell, J. C. Branca, D. L. Hughes and W. N. Olmstead, *J. Org. Chem.*, 1980, **45**, 3305–3313.
- R. R. Fraser, T. S. Mansour and S. Savard, *J. Org. Chem.*, 1985, **50**, 3232–3234.
- R. Dieter and W. Albert, *Isr. J. Chem.*, 1970, **8**, 259–271.
- J. W. Tucker and C. R. J. Stephenson, *J. Org. Chem.*, 2012, **77**, 1617–1622.
- L. Pause, M. Robert and J.-M. Savéant, *J. Am. Chem. Soc.*, 1999, **121**, 7158–7159.
- T. Koike and M. Akita, *Inorg. Chem. Front.*, 2014, **1**, 562–576.
- E. Prasad, B. W. Knettle and R. A. Flowers II, *Chem. Eur. J.*, 2005, **11**, 3105–3112.

TOC graphic:



A structural modification strategy to improve the photocatalytic performance of molecular cerium(III) luminophores was demonstrated.